Subwavelength-resolution photoacoustic microscopy for label-free detection of optical absorption in vivo

Chi Zhang, Konstantin Maslov, Lihong V. Wang

Chi Zhang, Konstantin Maslov, Lihong V. Wang, "Subwavelength-resolution photoacoustic microscopy for label-free detection of optical absorption in vivo," Proc. SPIE 7899, Photons Plus Ultrasound: Imaging and Sensing 2011, 78990L (17 February 2011); doi: 10.1117/12.873225

SPIE.

Event: SPIE BiOS, 2011, San Francisco, California, United States

Subwavelength-resolution photoacoustic microscopy for label-free detection of optical absorption *in vivo*

Chi Zhang, Konstantin Maslov, Lihong V. Wang*
Optical Imaging Laboratory, Department of Biomedical Engineering, Washington University in St. Louis, One Brookings Drive, St. Louis, MO 63130, USA
*Corresponding author: lhwang@biomed.wustl.edu

ABSTRACT

Mainstream optical microscopy technologies normally detect fluorescence or scattering, which may require undesirable labeling, but cannot directly sense optical absorption, which provides essential biological functional information. Here we reported *in vivo* and label-free subwavelength-resolution photoacoustic microscopy (SW-PAM) by using a water-immersion optical objective with a 1.23 NA. Capable of detecting nonfluorescent endogenous pigments, SW-PAM provides exquisitely high optical-absorption contrast. And, as a result of background-free detection, the sensitivity of SW-PAM to optical absorption reaches 100%. SW-PAM was demonstrated with wide-field optical microscopy by imaging gold nanospheres, *ex vivo* cells, and *in vivo* vasculature and melanoma. It was shown that SW-PAM has approached the ultimate diffraction-limited optical resolution—220 nm resolution at 532 nm wavelength. Subcellular organelles, such as melanosomes, can be resolved by SW-PAM. Vasculature and early-stage melanoma were imaged with 21:1 and 34:1 contrasts, respectively, without labeling. For all these applications, SW-PAM has contrasts orders of magnitude higher than wide-field optical microscopy. Therefore, SW-PAM is expected to join the mainstream microscopy technologies.

Keywords: photoacoustic microscopy, subwavelength-resolution, label-free

1. INTRODUCTION

Photoacoustic microscopy (PAM) is an emerging biomedical imaging technology that obtains an image of tissue by detecting acoustic signals induced by focused laser pulses [1–3]. PAM uses a different contrast mechanism than the common forms of optical microscopy (OM). Elastic-scattering OM—such as confocal microscopy or optical coherence tomography—detects backscattered photons and therefore images scattering contrast. Fluorescence OM—such as confocal microscopy or two-photon microscopy—detects inelastically scattered photons from samples, normally labeled by exogenous fluorescent markers, so the contrast is sensitive to the concentration of fluorophores and the fluorescence quantum yield [4,5]. However, for most endogenous pigments only a small amount of absorbed energy is converted to fluorescence, while most energy is converted to heat and subsequently induces photoacoustic signals. By detecting these signals, PAM is theoretically 100% sensitive to optical absorption, and so can provide essential biological functional information. In biological tissue, nonfluorescent melanin and hemoglobin are major sources of endogenous absorption in the visible and near-infrared spectral range. Accordingly, PAM's high sensitivity to endogenous contrast has resulted in successful imaging of melanoma [6] and tumor angiogenisis [7].

2. METHODS

Here we have achieved subwavelength-resolution PAM (SW-PAM)—220 nm resolution at 532 nm wavelength—by using a water-immersion optical objective with a 1.23 numerical aperture (NA) [8]. Approaching the diffraction limit, 220 nm is the highest resolution of PAM that has been reported. As shown in Fig. 1, SW-PAM utilized a Nd:YVO4 laser (532 nm wavelength) as the irradiation source. Laser pulses with a 1.5 ns duration were generated and transmitted to the optical objective through a single-mode optical fiber. The sample was irradiated by the laser pulse (typical energy was 10 nJ for slide samples and 60 nJ for mouse ears) focused by the objective. The resulting photoacoustic waves were detected by an ultrasonic transducer with a central frequency of 40 MHz and an NA of 0.5 in transmission mode. The signals

Photons Plus Ultrasound: Imaging and Sensing 2011, edited by Alexander A. Oraevsky, Lihong V. Wang,
Proc. of SPIE Vol. 7899, 78990L · © 2011 SPIE · CCC code: 1605-7422/11/$18 · doi: 10.1117/12.873225

were then amplified and digitized at a sampling rate of 1 GHz. To obtain a point-by-point maximum-amplitude projection (MAP) image, the objective and the transducer mechanically scanned in raster mode in the *x*-*y* plane, with a scanning speed of 2 mm/s and a step size of 125 nm.

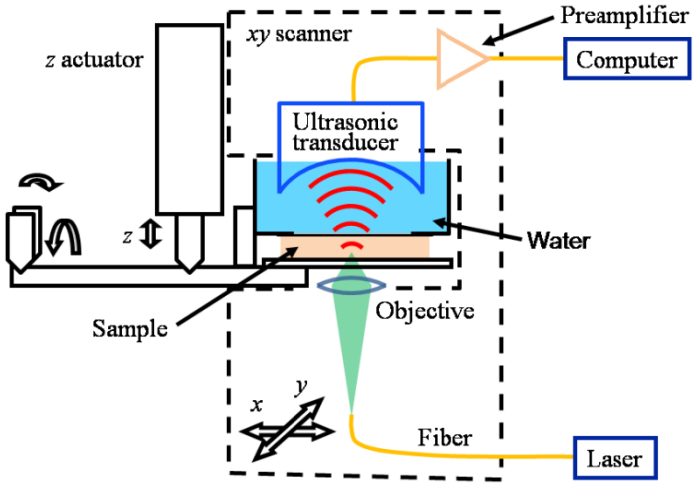

Figure 1. Schematic diagram of SW-PAM.

3. RESULTS

The transverse spatial resolution of SW-PAM was measured by imaging gold nanospheres with a diameter of 15 nm [Fig. 2(a)]. The nanospheres were ideal point absorbers to generate the point spread function (PSF) of SW-PAM. In the image, typical spheres were chosen and fitted by the theoretical Bessel-form function [Fig. 2(b)]. The system resolution, given by the full width at half maximum (FWHM) of the Bessel-form PSF, was quantified as 220 ± 20 nm, agreeing well with the theoretical value $0.51\lambda/\mathrm{NA} \approx 221$ nm.

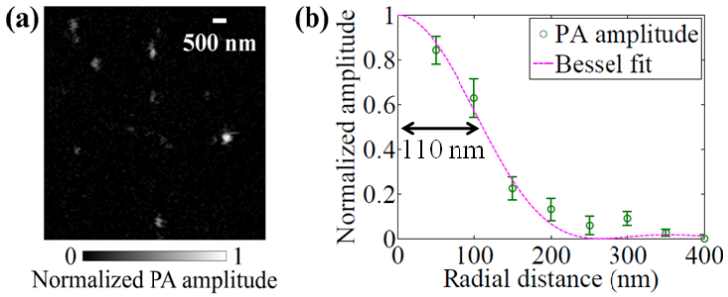

Figure 2. Measuring the transverse spatial resolution of SW-PAM. (a) Image of gold nanospheres. (b) Point spread function of the system. Circle: the averaged pixel value. Line: the theoretical Bessel-form function.

To validate SW-PAM with wide-field OM, we imaged *ex vivo* melanoma cells, red blood cells, and onion epidermal cells, as shown in Fig. 3. The PAM images have a dark background, while the OM images have a bright background. The bright (white) dots in the PAM image of melanoma cells are melanosomes—organelles containing melanin [Fig. 3(a), left]. However, the melanosomes appear dark in the OM image [Fig. 3(a), middle] because their absorption attenuated the light transmission. The PAM image has a contrast of (54.5±0.4):1 and a contrast-to-noise ratio (CNR) of 49 dB, while the OM image has a much lower contrast of (0.79±0.04):1 and a lower CNR of 25 dB. This difference is because PAM is sensitive only to absorption, but OM shows both absorption and scattering (the latter is relatively close between melanosomes and other areas). Nuclei are clearly imaged by PAM, which is confirmed by staining them with 4',6-diamidino-2-phenylindole and taking a fluorescence OM image [Fig. 3(a), right]. In comparison, it is difficult to

identify the nuclei in the OM image due to the low contrast. For typical red blood cells (RBCs), as shown in Fig. 3(b), the contrast disparity between PAM and OM can also be observed (the two images show different areas of the cell sample). The characteristic donut shape of RBCs is clearly shown by PAM. Moreover, rich contrasts are observed in the epidermal cells of purple onion by PAM [Fig. 3(c)].

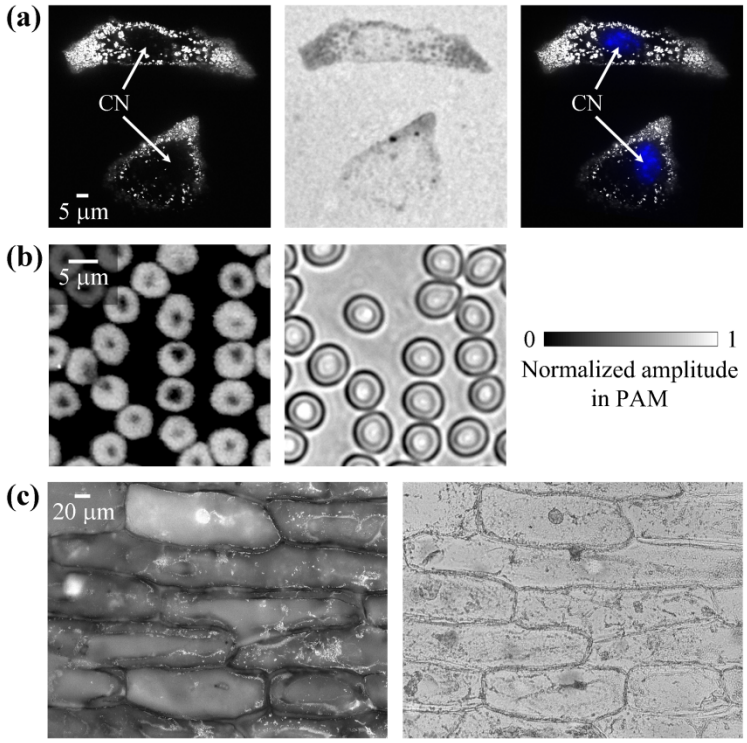

Figure 3. *Ex vivo* images of animal and plant cells. (a) Melanoma cells imaged by PAM, OM, and PAM plus the nuclei-stained (blue) fluorescence OM. CN: cell nucleus. (b) PAM and OM images of red blood cells. (c) PAM and OM images of onion epidermal cells.

Then we imaged mouse ears *in vivo* with SW-PAM. All experimental animal procedures were carried out in conformity with the laboratory animal protocol approved by the Animal Studies Committee of Washington University in St. Louis. We imaged the ear (depilated) of a black mouse (Harlan Co., C57BL/6NHsd, 25 g, male) in order to show the melanin distribution. Since most melanosomes reside in the basal layer of the epidermis, whose thickness is about 10 μm in this case [9], we acquired one image focusing at ~10 μm deep (Fig. 4). The single melanosomes (black dots) can be clearly identified. Deeper sebaceous glands can be observed, although slightly out of focus. Within this depth range we did not find an obvious decrease in resolution due to scattering. The OM image of the ear, although not shown here, has extremely low contrast. These results suggest potential applications of PAM in quantifying melanin distribution *in vivo*, which is important for detecting melanoma as well as determining individualized radiant exposure in dermatological laser therapies [10].

When imaging the ear of a nude mouse (Harlan Co., Hsd:Athymic Nude-Foxn1^{nu}, 30 g, male), we identified single RBCs *in vivo*. Here, we used an objective with a 0.60 NA (providing 400 nm resolution) instead because the thick layer of vessels required an extended focal zone. As shown in Fig. 5, all the blood vessels, including capillaries, were imaged with high contrast. Since nude mice do not have much melanin in their skin, the image has little background signal. Perhaps the blood vessel was damaged, so some RBCs came out. Motionless RBCs were imaged *in vivo*, and the characteristic donut shape of RBCS was clearly shown.

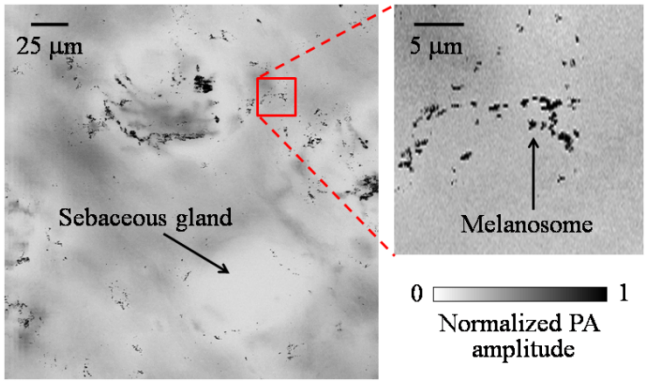

Figure 4. Melanin distribution in a black mouse ear *in vivo*.

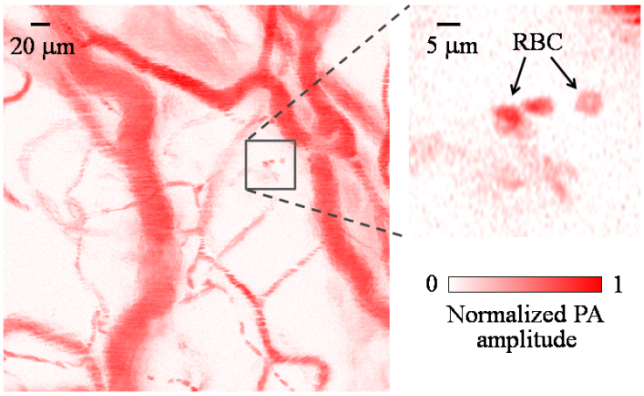

Figure 5. Mouse ear image where *in vivo* red blood cells (RBCs) can be identified (the close-up image indicates the biconcave structure of RBCs).

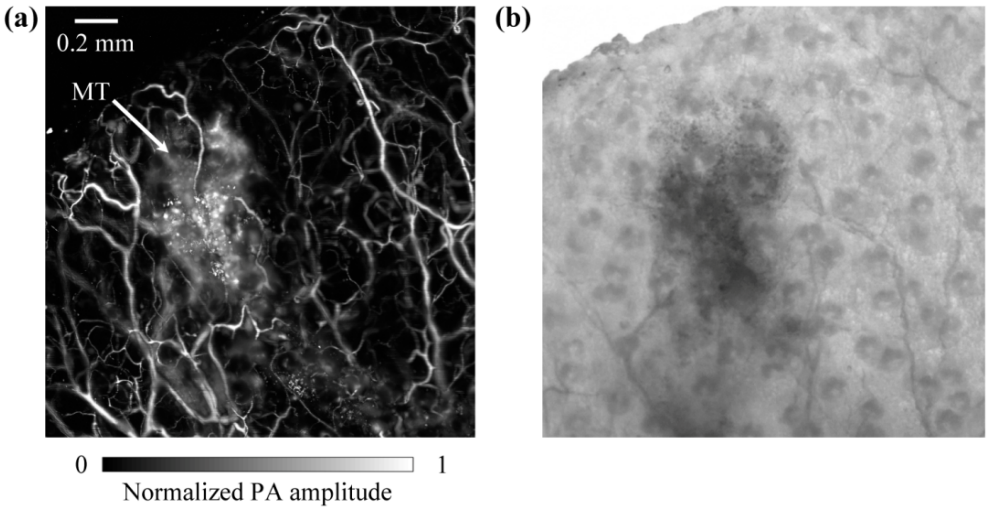

Figure 6. Monitoring of melanoma growing on a nude mouse ear. (a) PAM image of blood vessels and melanoma taken 3 days after injecting melanoma cells. MT: melanoma tumor. (b) OM image of the same area.

We monitored the melanoma growing on the ear of a nude mouse *in vivo*. 10 μl of suspension containing 1 million B16 melanoma cells was inoculated into the mouse ear. The ear was imaged by PAM 3 days later, as shown in Fig. 6(a). The melanoma generated stronger photoacoustic signals than the vessels and was easily identified. The vasculature and melanoma have contrasts of (21±4):1 (37 dB CNR) and (34±5):1 (41 dB CNR), respectively. In fact, their contrast difference can be further increased if we use other laser wavelengths (for example, 650 nm). In the wide-field OM image [Fig. 6(b)], the melanoma has a much lower contrast of (0.62±0.02):1 (26 dB CNR).

4. DISCUSSION AND CONCLUSIONS

In summary, structures as small as subcellular organelles can be resolved by SW-PAM for both *ex vivo* and *in vivo* imaging. Melanoma and vasculature can be visualized with high contrast. Therefore, SW-PAM has superior potential to detect melanoma in the early stage. Also, capable of imaging individual red blood cells *in vivo*, SW-PAM can potentially be used to count red blood cells as an *in vivo* flow cytometer, measure blood flow velocity in capillaries, and monitor sickle cell disease. The current transmission-mode configuration of SW-PAM limits the thickness of tissues that can be imaged. We are extending SW-PAM to reflection mode for applications in more anatomical sites. As a result, SW-PAM along with the scaled-up macroscopy—deep-penetrating photoacoustic tomography [11,12]—may bridge microscopic research and clinical practice, especially for melanoma detection, vasculature visualization, reporter gene imaging [13], and sentinel lymph node mapping [14].

ACKNOWLEDGEMENTS

We thank L. Li and Y. Wang for experimental assistance and helpful discussion, Y. Zhang for fixing and staining melanoma cells, D. Yao for help with optical microscopy, and M. Yang for preparing gold nanospheres. This work was sponsored in part by National Institutes of Health grants R01 EB000712, R01 EB008085, R01 CA113453901, U54 CA136398, and 5P60 DK02057933. L.W. has a financial interest in Microphotoacoustics, Inc. and Endra, Inc., which, however, did not support this work.

REFERENCES

[1] Wang, L. V., "Multiscale photoacoustic microscopy and computed tomography," Nature Photon. 3, 503–509 (2009).
[2] Zhang, H. F., Maslov, K., Stoica, G. and Wang, L. V., "Functional photoacoustic microscopy for high-resolution and noninvasive *in vivo* imaging," Nature Biotechnol. 24, 848–851 (2006).
[3] Laufer, J., Zhang, E., Raivich, G. and Beard, P., "Three-dimensional noninvasive imaging of the vasculature in the mouse brain using a high resolution photoacoustic scanner," Appl. Opt. 48, 299–306 (2009).
[4] Wang, L. V. and Wu, H., [Biomedical Optics: Principles and Imaging], Wiley, Hoboken, NJ, 1–14 (2007).
[5] Wang, Y., Maslov, K., Kim, C., Hu, S. and Wang, L. V., "Integrated photoacoustic and fluorescence confocal microscopy," IEEE Trans. Biomed. Eng. 57, 2576–2578 (2010).
[6] Gray-Schopher, V., Wellbrock, C. and Marais, R., "Melanoma biology and new targeted therapy," Nature 445, 851–857 (2007).
[7] McDonald, D. M. and Choyke, P. L., "Imaging of angiogenesis: from microscope to clinic," Nature Med. 9, 713–725 (2003).
[8] Zhang, C., Maslov, K. and Wang, L. V., "Subwavelength-resolution label-free photoacoustic microscopy of optical absorption *in vivo*," Opt. Lett. 35, 3195–3197 (2010).
[9] Kietzmann, K., Lubach, D. and Heeren, H.-J., "The mouse epidermis as a model in skin pharmacology: influence of age and sex on epidermal metabolic reactions and their circadian rhythms," Lab. Animal 24, 321–327 (1990).
[10] Verkruysse, W., Svaasand, L. O. and Franco, W., "Remittance at a single wavelength of 390 nm to quantify epidermal melanin concentration," J. Biomed. Opt. 14, 014005 (2009).
[11] Wang, X., Pang, Y., Ku, G., Xie, X., Stoica, G. and Wang, L. V., "Noninvasive laser-induced photoacoustic tomography for structural and functional *in vivo* imaging of the brain," Nature Biotechnol. 21, 803–806 (2003).

[12] Fronheiser, M. P., Ermilov, S. A., Brecht, H., Conjusteau, A., Su, R., Mehta, K. and Oraevsky, A. A., "Real-time optoacoustic monitoring and three-dimensional mapping of a human arm vasculature," J. Biomed. Opt. 15, 021305 (2010).
[13] Li, L., Zemp, R. J., Lungu, G., Stoica, G. and Wang, L. V., "Photoacoustic imaging of lacZ gene expression *in vivo*," J. Biomed. Opt. 12, 020504 (2007).
[14] Song, K. H., Stein, E. W., Margenthaler, J. A. and Wang, L. V., "Noninvasive photoacoustic identification of sentinel lymph nodes containing methylene blue *in vivo* in a rat model," J. Biomed. Opt. 13, 054033 (2008).